JACS
JOURNAL OF THE AMERICAN CHEMICAL SOCIETY

ARTICLE

pubs.acs.org/JACS

Hierarchically Controlled Helical Graphite Films Prepared from Iodine-Doped Helical Polyacetylene Films Using Morphology-Retaining Carbonization

Satoshi Matsushita,[†] Mutsumasa Kyotani,[‡] and Kazuo Akagi*[,†]

[†]Department of Polymer Chemistry, Kyoto University, Katsura, Nishikyo-ku, Kyoto 615-8510, Japan

[‡]Tsukuba Research Center for Interdisciplinary Materials Science, University of Tsukuba, Tsukuba, Ibaraki 305-8573, Japan

Supporting Information

ABSTRACT: One-handed helical graphite films with a hierarchically controlled morphology were prepared from iodine-doped helical polyacetylene (H-PA) films using the recently developed morphology-retaining carbonization method. Results from scanning electron microscopy indicate that the hierarchical helical morphology of the H-PA film remains unchanged even after carbonization at 800 °C. The weight loss of the film due to carbonization was very small; only 10−29% of the weight of the film before doping was lost. Furthermore, the graphite film prepared by subsequent heating at 2600 °C retained the same morphology as that of the original H-PA film and that of the helical carbon film prepared at 800 °C. The screwed direction, twisted degree, and vertical or horizontal alignment of the helical graphite film were well controlled by changing the helical sense, helical pitch, and orientation state of the chiral nematic liquid crystal (N*-LC) used as an asymmetric LC reaction field. X-ray diffraction and Raman scattering measurements showed that graphitic crystallization proceeds in the carbon film during heat treatment at 2600 °C. Transmission electron microscopy measurements indicate that ultrasonication of the helical graphite film in ethanol for several hours gives rise to a single helical graphite fibril. The profound potentiality of the present graphite films is exemplified in their electrical properties. The horizontally aligned helical graphite film exhibits an enhancement in electrical conductivity and an evolution of electrical anisotropy in which conductivity parallel to the helical axis of the fibril bundle is higher than that perpendicular to the axis.

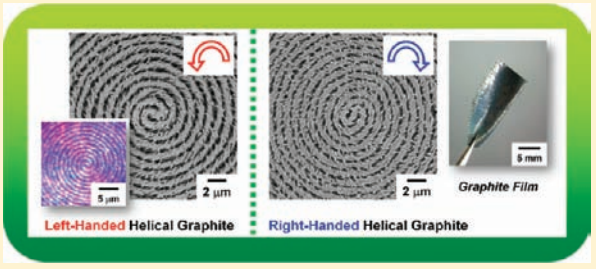

1. INTRODUCTION

Carbon materials have recently attracted considerable attention because of their versatile applicability in the fields of electronics, mechanics, transport, energy, and environmental science.[1,2] The carbon materials prepared from organic compounds are ordinarily in the form of bulk, particles, and fibers, such as carbon black and carbon fiber.[2] There are few carbon materials in the form of films, except for an evaporated carbon membrane supported by a substrate.[1] Carbon films and membranes are interesting materials because of their special mechanical and physicochemical properties as well as their chemical and thermal stabilities. They have been used in various applications, such as electrochemical energy storage,[1,3] fuel- and photovoltaic-cell electrodes,[4,5] field-effect transistors,[4,6] catalyst supports,[7] and wear-resistant coatings.[8] A large number of chemical approaches have been reported for preparing carbon films that consist of evaporated amorphous carbons,[3] graphene-based materials,[4,9] and randomly networked or macroscopically aligned carbon nanotubes (CNTs).[10] It is well-known that a freestanding graphite film can be prepared from an aromatic polymer film, such as a commercially available polyimide film, by carbonization and graphitization at high temperature and normal pressure.[2] However, it is difficult to prepare freestanding graphite films by the carbonization of organic polymer films in the desired form, especially in the form of a hierarchical nanostructure. This difficulty is because high-temperature carbonization causes thermal decomposition and volatilization of hydrocarbon gases, destroying the morphology of the original film.[11]

One-handed excess helical structures have also gained increasing interest due to their fruitful chiroptical properties. They are ordinarily composed of various organic materials, such as amphiphiles,[12] oligomers,[13] and nonconjugated[14] or conjugated polymers.[15] At the same time, these structures with highly twisted helices or superhelices are particularly desirable.[12e,15b] However, there are few helical structures in which helical carbon materials form hierarchical morphologies. Carbon films with peculiar structures, such as hierarchically controlled helical structures, are expected to afford novel chiroptical properties as well as electrical and electromagnetic properties. It is therefore intriguing to control the helical morphology of the carbon film to develop new carbon materials. To this end, an organic polymer film consisting of hierarchical helical fibrils may be suitable as a precursor for the carbon film.

Received: September 2, 2011
Published: October 04, 2011

dx.doi.org/10.1021/ja2082922 | J. Am. Chem. Soc. 2011, 133, 17977–17992

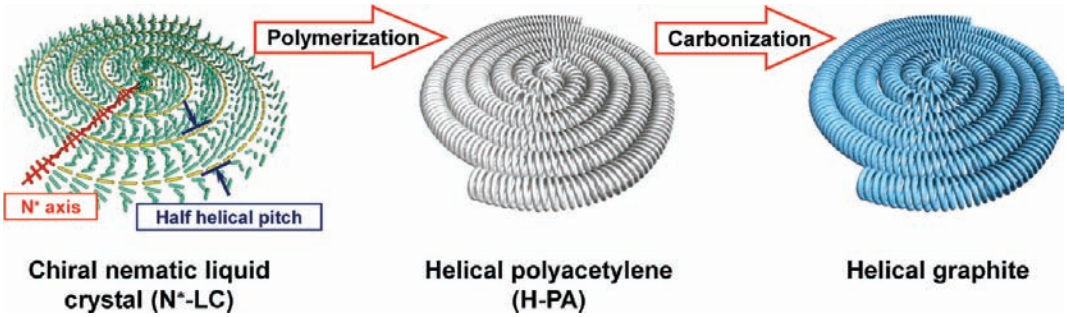

Figure 1. Schematic representation of the preparation of a helical graphite film with concentrically curled morphology using the carbonization of H-PA synthesized in a N*-LC field.

The liquid-crystal (LC) polymerization method using chiral nematic LC (N*-LC) as an asymmetric reaction field has enabled the preparation of an H-PA film in which bundles consisting of fibrils with diameters of approximately 100 nm are twisted and concentrically curled.[16] The N*-LC is prepared through the addition of a small amount of a chiral dopant into an N-LC.[17] This addition allows us to control the helical sense and helical power (helical pitch) of the N*-LC by selecting the chirality and helical twisting power (HTP; β_M) of the chiral dopant.[18] Because the N*-LC is composed of N-LC and a chiral dopant, such as an axially chiral compound with a (*R*)- or (*S*)-configuration, the screwed direction and twisted degree of the H-PA are rigorously controlled by tuning the chirality and HTP of the chiral dopant. Binaphthyl derivatives are useful in controlling the helical sense and helical pitch of the N*-LC, especially when their molecular structures are chemically modified by such methods as the introduction of mesogenic substituents into the binaphthyl rings.[16h]

Meanwhile, the macroscopic alignment of H-PA has also been successfully carried out using the N*-LC reaction field with a monodomain structure, which was constructed using gravity flow[19] or a magnetic field[20] as an external perturbation. A vertical-orientation inducer is useful for the construction of vertically oriented N*-LC reaction fields, allowing an orientation control without any external force.[21] The macroscopically oriented N*-LC produces vertically or horizontally aligned H-PA films.

From the viewpoint of evaluating physical, chiroptical, electrical, and electromagnetic properties, macroscopically aligned materials are favorable. Carbonization of H-PA films is one of the most promising ways to prepare a stable carbon film embodied with a peculiar structure if the precursor morphology is preserved during the carbonization even at high temperature.[22] Very recently, we developed a novel carbonization procedure using iodine-doped conjugated polymers as precursors, called "morphology-retaining carbonization". The iodine dopant reacts with the hydrogen atoms in the polymer chain, leading to the formation of hydrogen iodide (HI) gas during the carbonization heating. Consequently, this method enabled us to prepare carbon and graphitic films with completely preserved morphologies and even nanofibril structures.[23]

Here we present a comprehensive study of the morphology-retaining carbonization that produces helical carbon and graphite films with hierarchically controlled spiral and aligned morphologies based on H-PA precursors (Figure 1). First we show (i) left- and right-handed H-PA films with a multidomain spiral morphology that were synthesized in N*-LCs and (ii) macroscopically aligned H-PA films with monodomain spiral morphology that were synthesized in oriented N*-LCs. Next, we show (iii) left- and right-handed helical carbon films with spiral and vertically aligned morphologies, where the distances of the fibril bundle intrinsically depend on the HTPs of the chiral dopants in the N*-LCs used for the synthesis of H-PAs. Finally, we show (iv) left- and right-handed helical graphite films with macroscopically aligned morphologies. Special emphasis is laid on the fact that the carbon and graphite films are well controlled in terms of morphology and helicity despite the intrinsic difficulty in the fabrication of morphology and helical structures.

2. EXPERIMENTAL SECTION

Synthesis and Preparation of N*-LCs. Scheme 1 depicts the molecular structures of the chiral dopants, the vertical-orientation inducer, and the N-LCs. Di- and tetra-substituted axially chiral binaphthyl derivatives were synthesized as described in a previous report.[16,24] The former has LC substituents at the 2,2′ positions of the binaphthyl rings, (*R*)- or (*S*)-2,2′-PCH506-1,1′-binaphthyl [abbreviated as (*R*)- or (*S*)-D1];[16] the latter has LC substituents at the 2,2′ and 6,6′ positions of the binaphthyl rings, (*R*)- or (*S*)-2,2′-6,6′-PCH506-1,1′-binaphthyl [abbreviated as (*R*)- or (*S*)-D2][24] and (*R*)- or (*S*)-2,2′-PCH5012-6,6′-PCH5-1,1′-binaphthyl [abbreviated as (*R*)- or (*S*)-D3].[16f] The vertical-orientation inducer with an octamethylene chain, 1,8-bis-[(*trans*-4-*n*-pentylcyclohexyl)phenoxy]octane [$(PCH50)_2$8], was synthesized according to the previous work.[21] The N-LCs, *p*-(*trans*-4-*n*-propylcyclohexyl)ethoxybenzene (PCH302), *p*-(*trans*-4-*n*-propylcyclohexyl)butoxybenzene (PCH304), and *p*-(*trans*-4-*n*-pentylcyclohexyl)-hexyloxybenzene (PCH506), were synthesized using a method similar to that for $(PCH50)_2$8.

Table 1 summarizes the HTPs of the chiral dopants, the concentration ratios, and the helical pitches of the N*-LCs. The N*-LC of system 1 was prepared by adding 2 mol % of the chiral dopant, D1, into an equimolar mixture of the N-LCs, PCH302 and PCH304. The N*-LC of system 2 was prepared by adding 0.5 mol % of D2 into the N-LC. The N*-LC of system 4 was prepared by adding 3 mol % of D3 into the N-LC. The vertically oriented N*-LC of system 3 was prepared by adding 3 mol % of the vertical-orientation inducer, $(PCH50)_2$8, and 0.5 mol % of D2 into the N-LC, PCH506. The phenylcyclohexyl (PCH) substituent in the D1−D3 enhances the miscibility between the N-LC mixture and the binaphthyl derivative used as the chiral dopant. It is important to note that the liquid crystallinity of D2 and D3 contributes the miscibility.[21c] The high miscibility of the chiral dopant allows the increase of the concentration of the chiral dopant for the construction of highly twisted N*-LC and the widening of the temperature region of the N*-LC phase. A wide range of temperatures for the N*-LC is favorable for the acetylene polymerization because the heat produced during the polymerization reaction raises the temperature inside a Schlenk flask, easily destroying

Scheme 1. Components of (*R*)- and (*S*)-N*-LC Systems: Chiral Dopants, Vertical Orientation Inducer, and Nematic LCs (N-LCs)

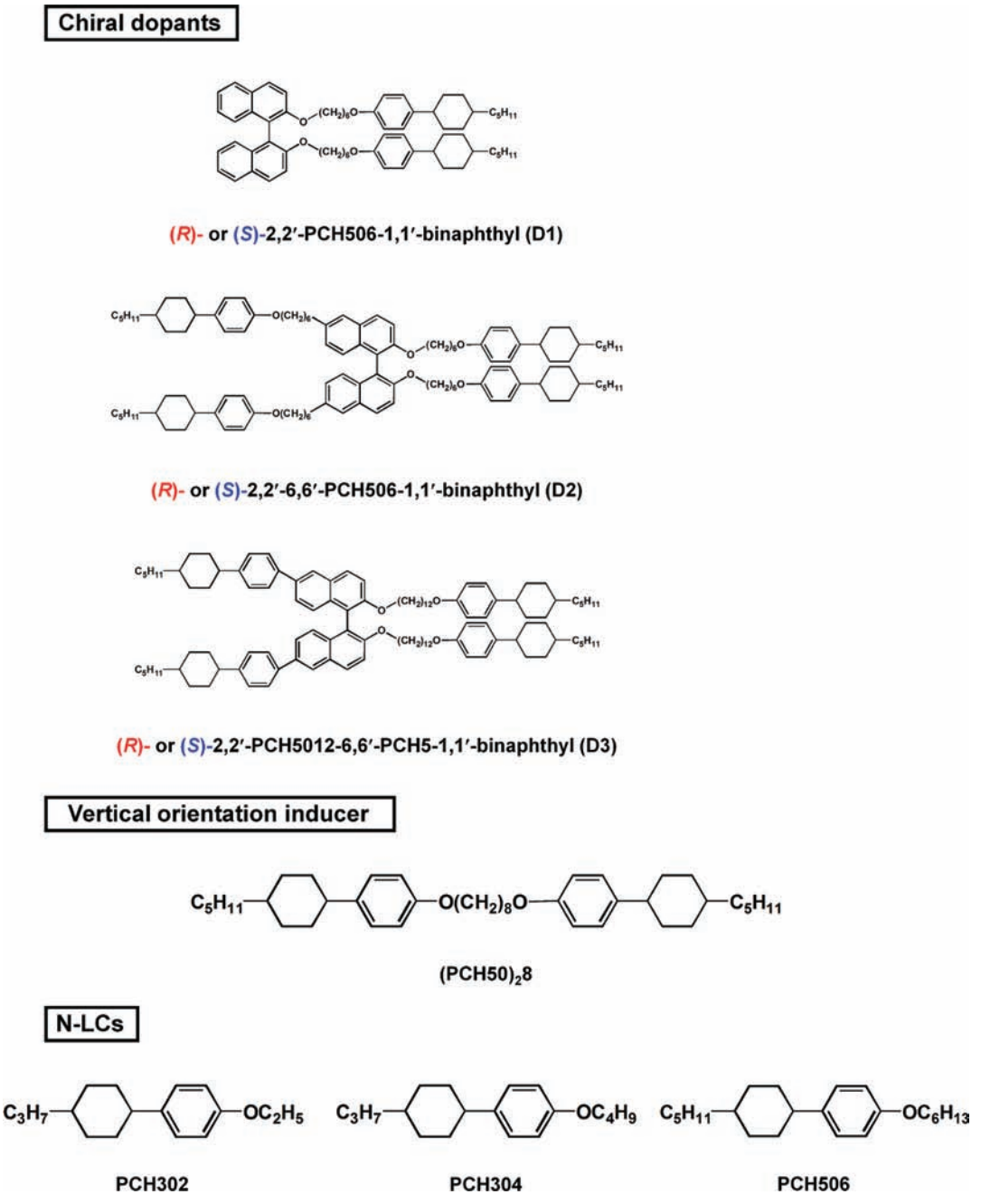

the LC phase into an isotropic phase. Therefore, the high miscibility achieved by the PCH substituent and the liquid crystallinity of the chiral dopants, in addition to the high HTPs, are important factors in the preparation of highly twisted N*-LCs.

3. RESULTS AND DISCUSSION

3.1. Characterization of N*-LCs. The helical senses of the N*-LCs were determined using the miscibility test (contact method).[25] This method is based on the observation of the mixing area between the N*-LC and the standard LC using a polarizing optical microscope (POM). Cholesteryl oleyl carbonate is known to be a left-handed N*-LC (cholesteric LC) at room temperature, and therefore it is useful as a standard for the miscibility test. If the helical sense of the N*-LC is the same as that of the standard LC, the mixing area will be continuous. Otherwise, it will be discontinuous (shown as a Schlieren texture of the N-LC). The miscibility tests indicate that the N*-LCs induced by (*R*)-chiral and (*S*)-chiral dopants have right- and left-handed screw structures, respectively.

In the POM image of system 1, which is a mixture of PCH302, PCH304, and (*R*)-2,2′-PCH506-1,1′-binaphthyl [(*R*)-D1], a fingerprint texture that is characteristic of the N*-LC phase is observed (Figure 2a). The distance between the striae corresponds

dx.doi.org/10.1021/ja2082922 |*J. Am. Chem. Soc.* 2011, 133, 17977–17992

Table 1. Helical Twisting Powers (HTPs) of Chiral Dopants, Concentration Ratios, and Helical Pitches of N*-LCs

chiral dopants					N*-LCs			
		rigidity[a]	helical twisting power; β_M (μm^{-1})[b]	liquid crystallinity[c]	system	mole ratios between components of N*-LCs	helical pitch (μm)[d]	orientation state
di-substituted	D1	low	*R*: 46	no	1	PCH302:PCH304:(*R*)- or (*S*)-D1 = 100:100:2	*R*: 2.2	horizontal
			S: 46				*S*: 2.2	
tetra-substituted	D2	low	*R*: 154	yes	2	PCH302:PCH304:(*R*)- or (*S*)-D2 = 100:100:0.5	*R*: 2.6	horizontal
			S: 160				*S*: 2.5	
			R: 87[e]		3	PCH506:$(PCH50)_2$8:(*R*)- or (*S*)-D2 = 100:3:0.5	*R*: 2.3	vertical
			S: 83				*S*: 2.4	
	D3	high	*R*: 256	yes	4	PCH302:PCH304:(*R*)- or (*S*)-D3 = 100:100:3	*R*: 0.26	Horizontal
			S: 247				*S*: 0.27	

[a] Rigidity in terms of linkages between the 6,6′ positions of the binaphthyl rings and the PCH moieties. [b] The HTP of the chiral dopant, i.e., the ability to convert host N-LC into N*-LC, was evaluated in N-LC of the equimolar two mixture of PCH302 and PCH304 using, $\beta_M = (pcr)^{-1}$, where p is the helical pitch in micrometers, c is the molar concentration of the chiral dopant in the N*-LC represented as (mole of chiral dopant)/(mole of PCH302 + mole of PCH304), and r is the enantiomeric purity of the chiral dopant; here, r is assumed to be 1. [c] Liquid crystallinity of chiral dopant itself. [d] The helical pitches of N*-LCs [systems 1−3] were precisely evaluated by measuring the distance between Cano lines appearing on the surface of a wedge-type cell under the POM at polymerization temperature.[16c,26] Meanwhile, when the helical pitch was smaller than 1 μm [system 4], it was evaluated with the selective light reflection method. The helical pitch was evaluated according to the equation, $p = \lambda_{max}/n$, where λ_{max} is the center wavelength for the maximally reflected light, and n is the mean refraction index of N*-LC ($n \cong 1.5$).[27] [e] The HTP was evaluated in N-LC of PCH506. The molar concentration c is represented as (mole of chiral dopant)/(mole of PCH506).

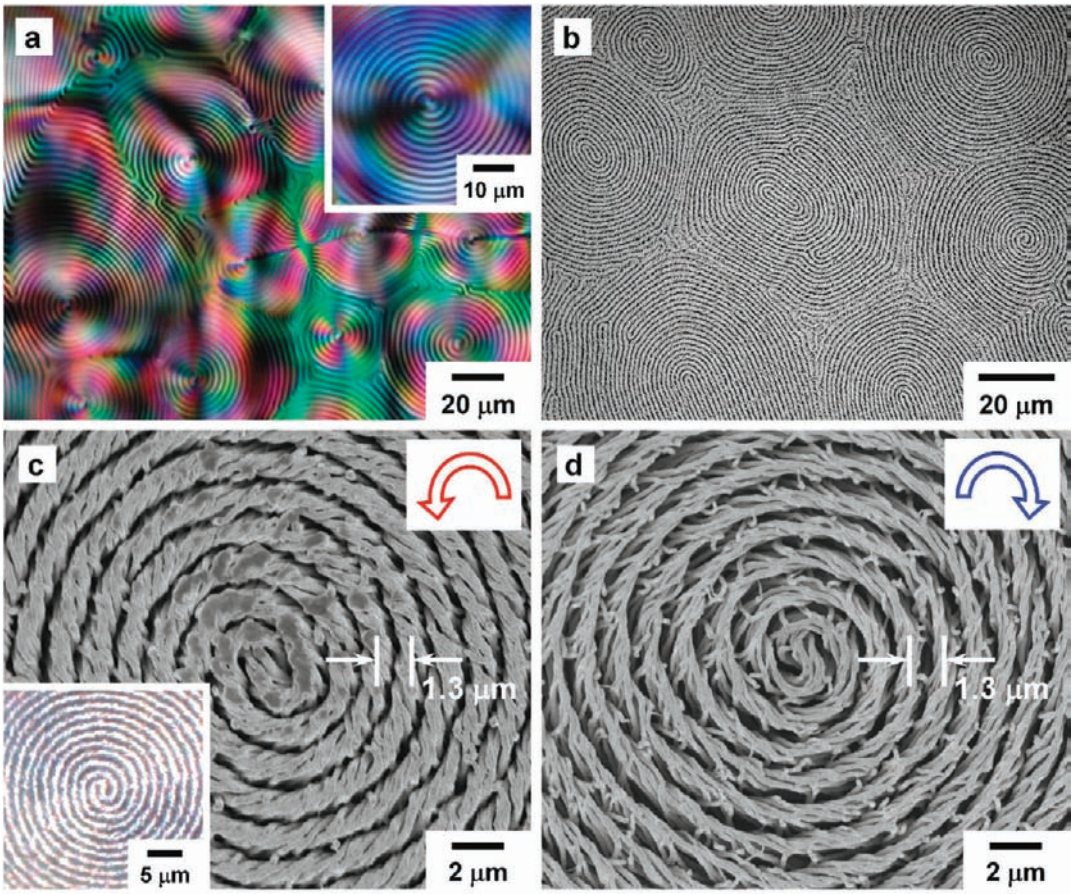

Figure 2. (a) POM image of the mixture of PCH302, PCH304, and (*R*)-2,2′-PCH506-1,1′-binaphthyl [system 1; PCH302:PCH304:(*R*)-D1 = 100:100:2 (mol %)] with a multidomain texture at 10 °C in the cooling process. The inset shows a magnified image of the POM. (b) SEM image of the H-PA film with a multidomain morphology synthesized in the (*R*)-N*-LC of system 1. SEM images of (c) left- and (d) right-handed H-PA films with spiral morphologies synthesized in N*-LC using the (c) (*R*)- and (d) (*S*)-D1 of system 1, respectively. The inset shows the DICM image of the left-handed H-PA film.

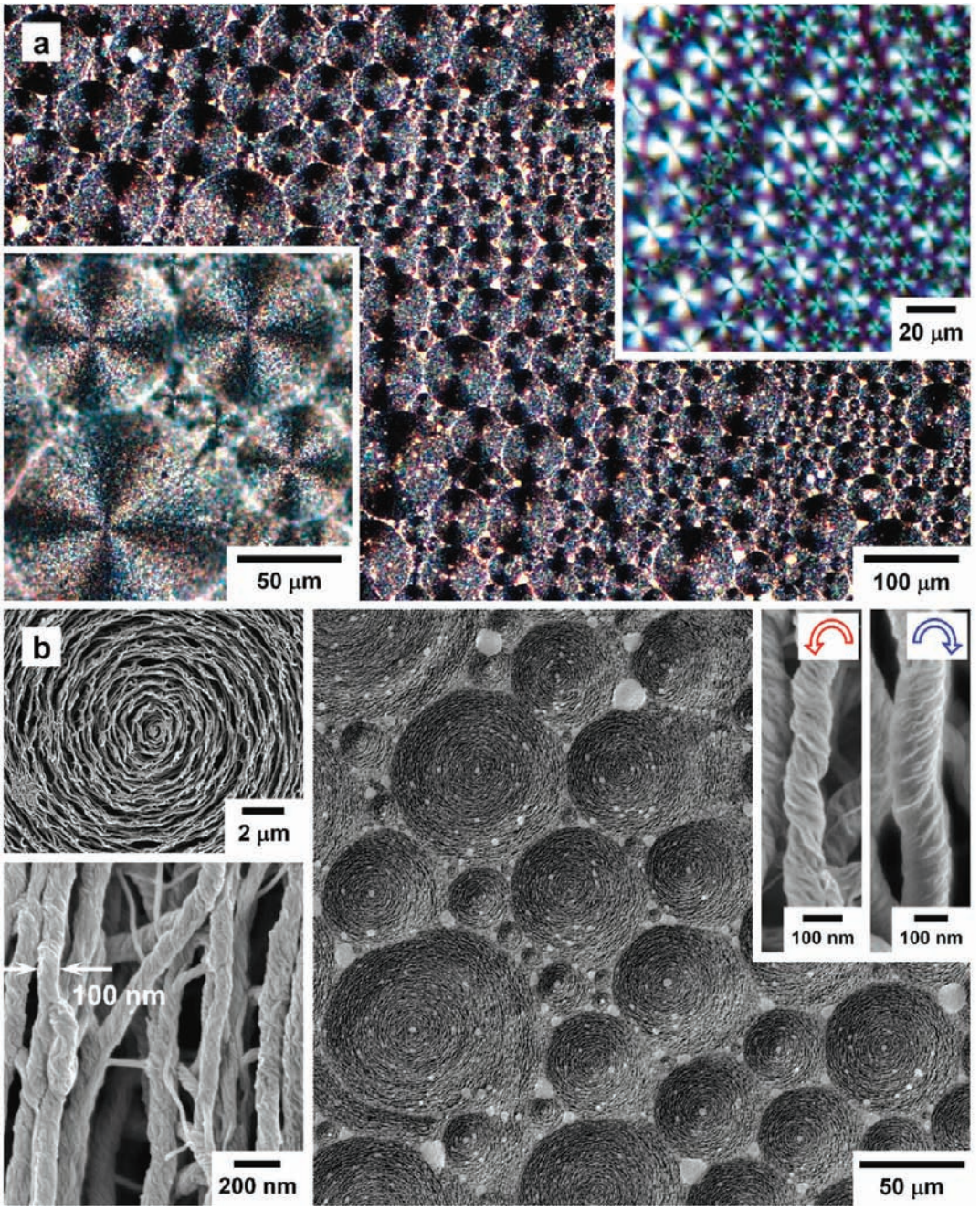

Figure 3. (a) DICM image of a highly twisted H-PA film with a multidomain morphology synthesized in the (*R*)-N*-LC of system 4. The upper-right inset shows the POM image of the mixture of PCH302, PCH304, and (*S*)-2,2′-PCH506-6,6′-PCH5-1,1′-binaphthyl [system 4; PCH302:PCH304:(*S*)-D3 = 100:100:3 (mol %)] with a multidomain texture at 20 °C in the cooling process. The lower-left inset shows the spherulitic domains of the H-PA film. (b) SEM image of the H-PA film, which is magnified in the upper-left inset. The lower-left inset shows the SEM image of the single helical fibrils. The upper-right inset shows the SEM images of the left- and right-handed helical fibrils, respectively.

to the half-helical pitch of the N*-LC. The N*-LC phase was observed in the temperature range of 17−33 °C and −16−32 °C during the heating and cooling processes, respectively. In systems 2 and 3, a texture similar to that of system 1 is observed. The N*-LC phase of system 2 was observed in the temperature range of 17−34 and −11−33 °C during the heating and cooling processes, respectively. Note that system 3 is a vertically oriented N*-LC because it includes $(PCH50)_2 8$ as a vertical-orientation inducer. The vertically oriented N*-LC phase was observed in the temperature range of 33−49 °C and 34−49 °C during the heating and cooling processes, respectively.

By contrast, in the POM image of system 4, which is the mixture of PCH302, PCH304, and (*S*)-2,2′-PCH5012-6,6′-PCH5-1,1′-binaphthyl [(*S*)-D3], a fan-shaped focal conic texture is observed, but no striae characteristic of N*-LC phase are seen (Figure 3a, inset). This lack of observed striae is due to the fact that the distance between the striae is too short to be detected in the POM. Note that as the degree of twist in the N*-LC increases, the helical pitch observed with POM decreases. The N*-LC

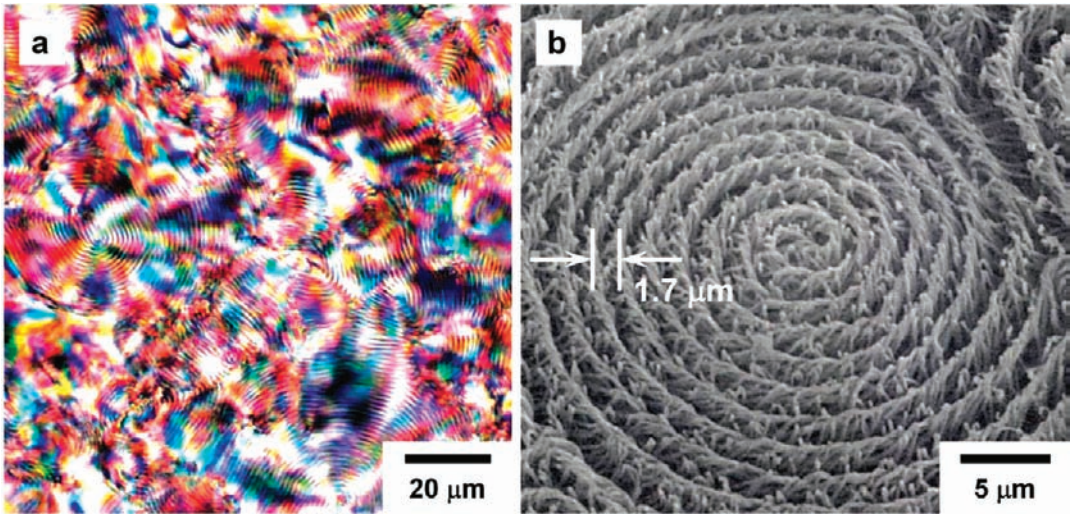

Figure 4. (a) POM image of the vertically oriented N*-LC field at 39 °C in the cooling process, which is the mixture of PCH506, $(PCH50)_28$, and (*R*)-2,2′-6,6′-PCH506-1,1′-binaphthyl [system 3; PCH506:$(PCH50)_28$:(*R*)-D2 = 100:3:0.5 (mol %)] including the Ziegler−Natta catalyst. (b) SEM image of the left-handed H-PA film with vertically aligned morphology synthesized in the (*R*)-N*-LC of system 3.

phase was observed in the temperature range of 16−37 °C and −12−37 °C during the heating and cooling processes, respectively. This sufficiently wide temperature region enabled us to perform the acetylene polymerization in the N*-LC phase.

The helical pitches of systems 1−3 (including D1 and D2) were evaluated using Cano's wedge method.[16c,26] This method is based on the observation of the distance between the discontinuity lines that appear when the N*-LC is inserted into a cell with a thickness gradient. The helical pitches of the N*-LCs of system 1−3 are 2.2, 2.5−2.6, and 2.3−2.4 μm, respectively (Table 1).

In contrast, the helical pitch of system 4 (including D3) was evaluated using the selective light-reflection method because the helical pitch of system 4 is too short to be observed using the Cano's wedge method. The center wavelength for the maximally reflected light (λ_{max}) was 390−405 nm. Thus, the helical pitch of system 4 was evaluated as 260−270 nm using the equation $p = \lambda_{max}/n$ ($n \cong 1.5$).[27]

The HTPs of D1 and D2 are 46 and 154−160 μm^{-1}, respectively. It is clear that the HTP of the chiral dopant D2 is approximately 3 times larger than that of D1. This difference can be rationalized by the difference in the number of substituents. Namely, the axially twisting torque of D2 is more effectively transferred to the parent N-LC because of the interactions between the four PCH substituents of D2 and the PCH moieties of LC molecules, whereas D1 bears only two PCH substituents.

In addition, the HTP of D3 is 247−256 μm^{-1}, which is 1.5−1.7 times larger than that of D2 (154−160 μm^{-1}). The structural difference between D2 and D3 is that the PCH moieties are indirectly and directly linked with the 6,6′ positions of the binaphthyl rings, respectively. That is, the absence of the hexamethylene spacer [-$O(CH_2)_6$-] in D3 leads to a rigidity in the linkage between the PCH moieties and the binaphthyl rings, resulting in a larger HTP than in the case of D2.

3.2. Morphologies of H-PA Films. Concentrically curled and vertically or macroscopically aligned H-PA films were synthesized through interfacial acetylene polymerizations in asymmetric reaction fields consisting of the N*-LC systems and the Ziegler−Natta catalyst tetra-*n*-butoxytitanium, Ti(O-*n*-Bu)$_4$, and triethylaluminum, $AlEt_3$. The full experimental details of the polymerization methods are in the Supporting Information. Figure 2b−d show scanning electron microscope (SEM) and differential-interference contrast microscope (DICM) images of the concentrically curled H-PA films synthesized using the N*-LC of system 1 with a helical pitch of 2.2 μm. The SEM images show the formation of a large domain of spiral morphology that is composed of a helical structure of a bundle of fibrils with a one-handed screw direction. The hierarchical helical morphology of the H-PA replicates that of the N*-LC during an interfacial acetylene polymerization (insets of Figure 2a and c). The H-PA is lying on the surface, i.e., the helical axis of the PA fibril bundle is parallel to the film surface. The distance between the fibril bundles is almost half of the helical pitch in the N*-LC, and the screw directions of the spiral and the fibril run opposite to the helical senses of the N*-LCs.[16c−e]

In contrast, Figure 3a shows the spherulitic multidomain morphology of the highly twisted H-PA film synthesized using the ultimately screwed (*R*)-N*-LC of system 4 (Figure 3a, inset) with a helical pitch as narrow as 260 nm. The DICM and SEM images of the H-PA films show that many spiral domains exist in the film and that the single fibrils screwed in the left- or right-hand directions form the spiral domains (Figure 3).

Figure 4b shows an SEM image of the vertically aligned H-PA film synthesized using the (*R*)-N*-LC of system 3 (Figure 4a). The fibril bundles of the H-PA are vertically aligned and highly twisted in the left-hand direction. The helical axis of the fibril bundle is perpendicular to the film surface.[21c] This finding is in contrast to the case of the concentrically curled H-PAs synthesized in the N*-LCs of systems 1, 2, and 4, where the helical axis is parallel to the film surface (Figure 1).

Horizontally aligned H-PA films were synthesized via acetylene polymerization in the N*-LC reaction field composed of system 1 or 2 with a monodomain structure. The monodomain of the LC phase was prepared by gravity flow as an external perturbation to the N*-LC. The POM results indicate that the N*-LC aligns from a multidomain to a monodomain structure under an applied gravity flow, giving rise to an anisotropic field (Figure 5a, inset). The N*-LC exhibits an aligned optical texture in which the direction of the striae is parallel to that of the gravity

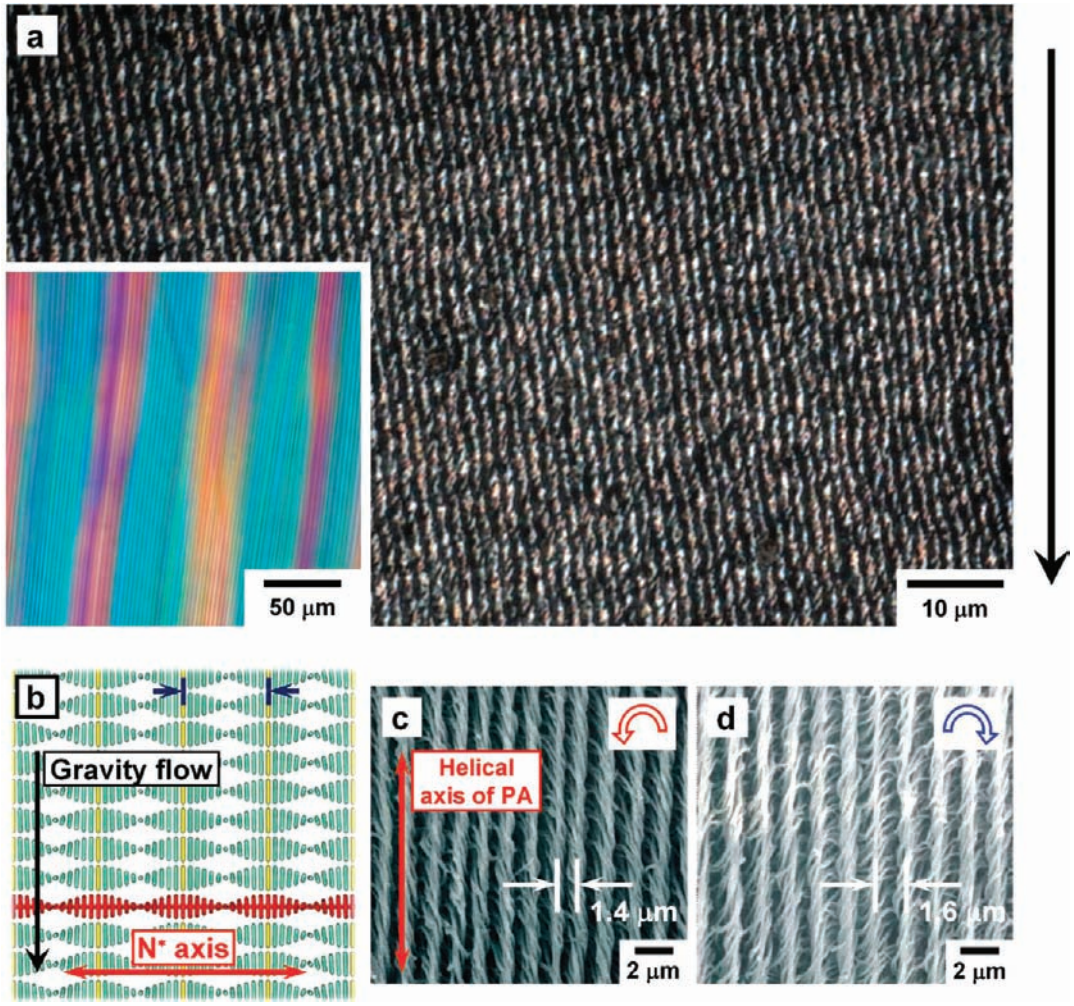

Figure 5. (a) DICM image of the horizontally aligned H-PA film synthesized in the (*S*)-N*-LC of system 1. The inset shows the POM image of the free surface of horizontally oriented (*S*)-N*-LC under gravity flow at 10 °C in the cooling process. The arrow indicates the direction of the gravity flow. (b) Schematic representation of the horizontally oriented N*-LC. SEM images of the left- (c) and (d) right-handed H-PA films with horizontally aligned morphologies synthesized in N*-LC using (c) (*R*)- and (d) (*S*)-D2 [system 2], respectively.

of flow. Thus, the helical axis of the N*-LC aligns perpendicularly to the direction of the gravity of flow, while the helical pitch of N*-LC remains unchanged after applying the gravity flow (Figure 5b). Note that the half-helical pitch of the aligned N*-LC (1.1 μm) was same as the half-helical pitch of the spiraled N*-LC (1.1 μm) (insets of Figures S1a and S1c in Supporting Information). Namely, the chirality of the N*-LC remains preserved even after the application of the gravity flow. It is therefore expected that the interfacial acetylene polymerization in the asymmetric reaction field constructed with the aligned N*-LC field gives a uniaxially aligned H-PA film, as seen in Figure S1d in Supporting Information.

Figure S2a in Supporting Information shows a photograph of the aligned H-PA film synthesized in an N*-LC using the gravity-flow technique. The aligned H-PA film exhibits a dull metallic luster. It shows a linearly polarized dichroism when the polarizer is arranged parallel (bright) or perpendicular (dark) to the aligned direction of the H-PA film (Figure S2b in Supporting Information). The DICM and SEM images of the H-PA films synthesized in the N*-LCs of systems 1 and 2 using the gravity-flow technique are shown in Figure 5. These images show that the helically screwed fibril bundles are well aligned parallel to the direction of gravity flow. Thus, the helical axis of the PA fibril bundle is perpendicular to that of the N*-LC.[16c−e] The orthogonal relationship in the helical axis between the fibril bundle and N*-LC holds, which is irrespective of the orientation state of N*-LC. The distance between the fibril bundles (1.0−1.1 μm) is almost the same as the half-helical pitch of the aligned N*-LC (1.1 μm) (Table 1 and Figure S3 in Supporting Information). It is worth noting that the aligned H-PA film synthesized in the (*R*)-N*-LC of system 1 showed anisotropy in electrical conductivity, where the conductivity parallel ($\sigma_{\parallel}$) to the helical axis of the fibril bundle is higher than that perpendicular ($\sigma_{\perp}$) to it. The electrical conductivities were measured using the four-probe method. Maximum values of parallel and perpendicular conductivities were 6.4×10^3 and 2.8×10^3 S/cm, respectively. Figure S4 in Supporting Information shows changes of parallel ($\sigma_{\parallel}$) and perpendicular ($\sigma_{\perp}$) conductivities during vapor phase iodine doping, giving an anisotropic ratio (defined as $\sigma_{\parallel}/\sigma_{\perp}$) of 2.3.

Figure S5 in Supporting Information shows a schematic representation of the synthesis of an aligned H-PA film using a gravity-flow technique. The N*-LC containing the catalyst macroscopically aligns from a multidomain to a monodomain structure under an applied gravity flow in a few minutes of

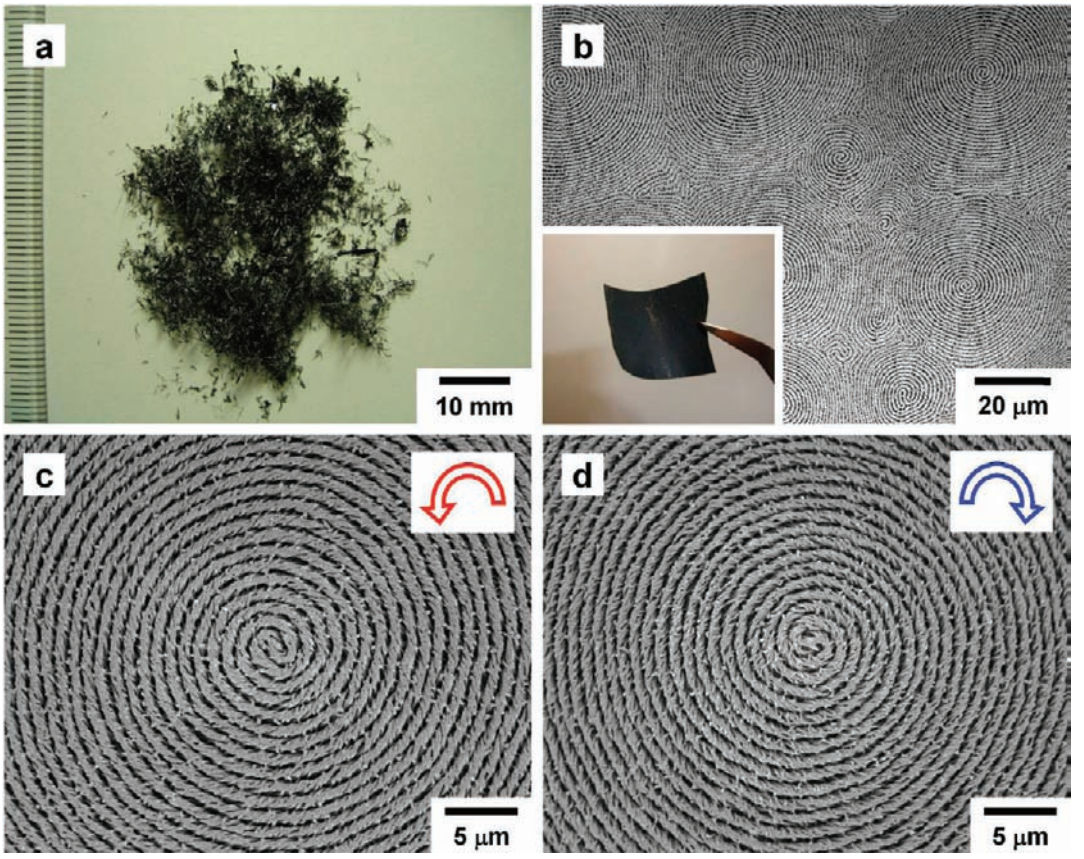

Figure 6. (a) Photograph of the carbon particles. The carbon particles were prepared from the pristine PA film at 800 °C. Elemental analysis exhibited that the film has hydrogen content of 1.4 wt %. (b) SEM image of the helical carbon film with multidomain spiral morphology prepared from an iodine-doped H-PA film at 800 °C using the (*R*)-N*-LC of system 1. The inset shows the flexible freestanding carbon film. SEM images of (c) left- and (d) right-handed helical carbon films with spiral morphologies prepared at 800 °C for H-PAs that are synthesized in N*-LC using (c) (*R*)- and (d) (*S*)-D1 [system 1], respectively.

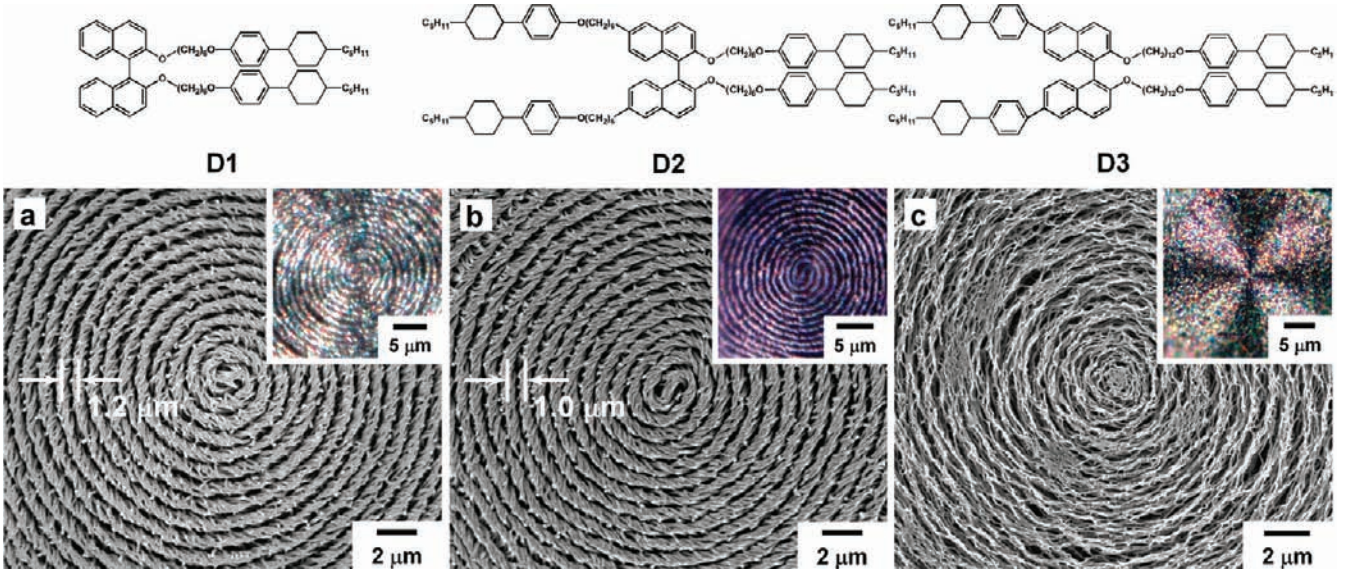

Figure 7. SEM images of the helical carbon films with spiral morphologies prepared at 800 °C using N*-LCs including (a) (*S*)-D1 [system 1], (b) (*S*)-D2 [system 2], and (c) (*R*)-D3 [system 4]. The insets show the DICM images of the helical carbon films.

orientation time, giving rise to an anisotropic reaction field. The interfacial acetylene polymerization in the anisotropic reaction field constructed with the aligned N*-LC field gives a uniaxially aligned H-PA film. The H-PA film thus obtained is completely

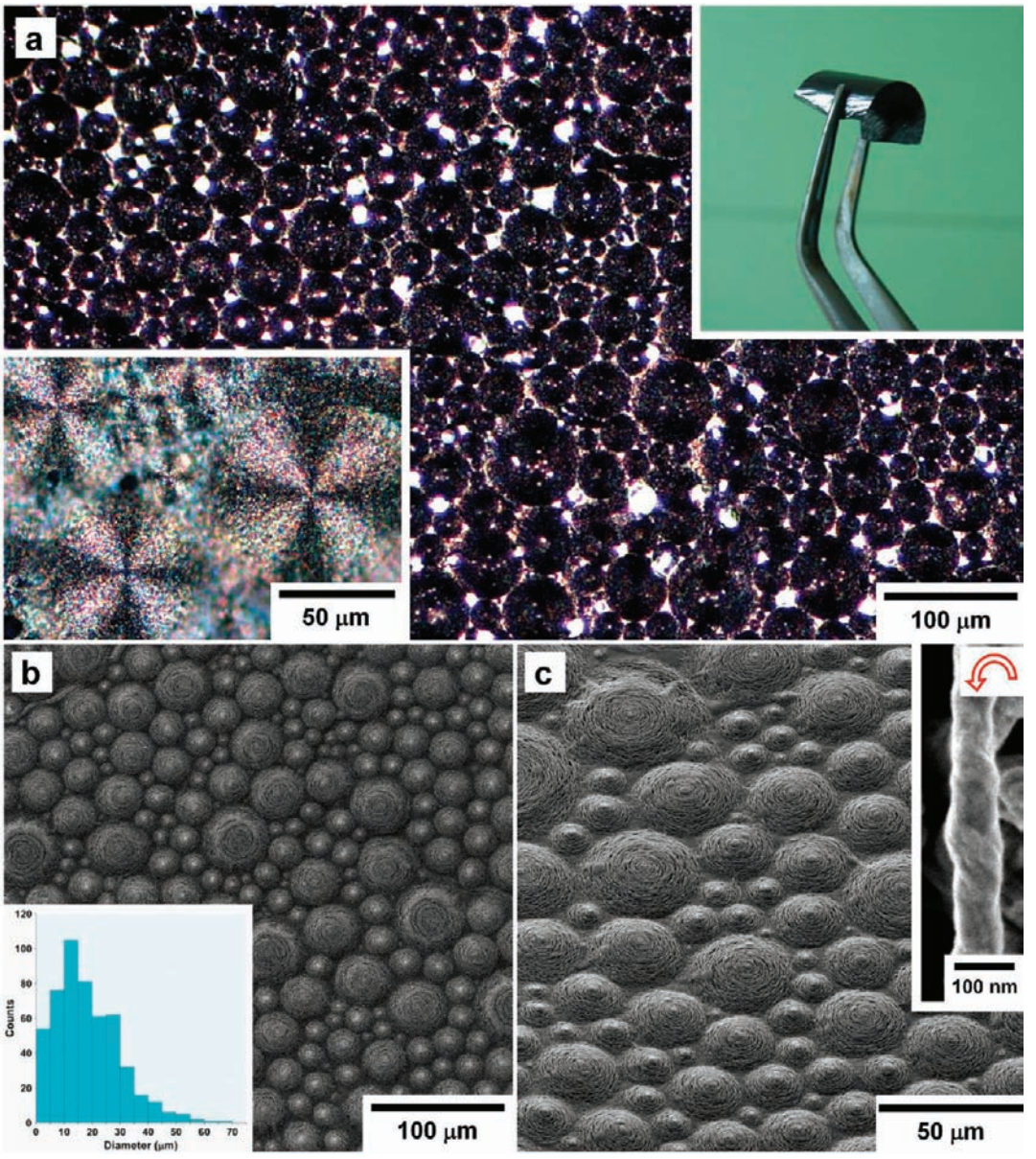

Figure 8. (a) DICM image of a highly twisted helical carbon film with a multidomain morphology prepared by the morphology-retaining carbonization of an iodine-doped H-PA film at 800 °C using (*R*)-N*-LC [system 4]. The insets show the flexible freestanding carbon film (upper right) and its spherulitic domains (lower left). (b) Top-view SEM image of the carbon film. The inset shows a diameter distribution histogram of the multidomain. (c) Isometric-view SEM image of the carbon film. The inset shows the SEM image of the left-handed helical carbon fibril.

washed with organic solvents for the removal of the catalyst solution consisting of the LC mixture. The aligned H-PA film has aligned helical bundles of fibrils parallel to the direction of the gravity flow that are free from spiraled morphology.

3.3. Iodine Doping, Carbonization, and Graphitization. Iodine doping was performed by exposing the H-PA film to iodine gas at room temperature for 24 h in a glass vessel. The amount of doped iodine was determined by weighing the doped H-PA films. The atomic ratio of doped iodine to carbon in the H-PA film (I/C) was 0.26−0.30. These results indicate that a fully doped H-PA film was used for the carbonization. The doped H-PA film was placed between graphite plates (80 × 80 × 2 mm) and was inserted into an electric furnace (KDF75, Denken). The doped H-PA film was then carbonized at 800 °C using the electric furnace for 1 h under flowing argon gas. The prepared carbon film was furthermore heated at 2600 °C for 30 min with a graphitizing apparatus (Sanriko denki) under flowing argon gas. The hydrogen contents of the carbon films after carbonization and graphitization were less than 1.0 and 0.5 wt %, respectively. The bulk densities of the helical carbon films prepared using the (*S*)-N*-LC of system 1 after carbonization and graphitization were 0.59 and 0.39 g/cm^3, respectively.

3.4. Morphologies of Helical Carbon Films. As shown in inset of Figure 6b, the freestanding carbon film was prepared from the iodine-doped H-PA film by the carbonization at 800 °C (Figures S6 and S7 in Supporting Information). The carbonization was confirmed by the elemental analysis of the film. Interestingly, the hierarchical helical morphology of the H-PA film remains unchanged after the carbonization. Figures 6b−d and 7a show the SEM images of helical carbon films prepared

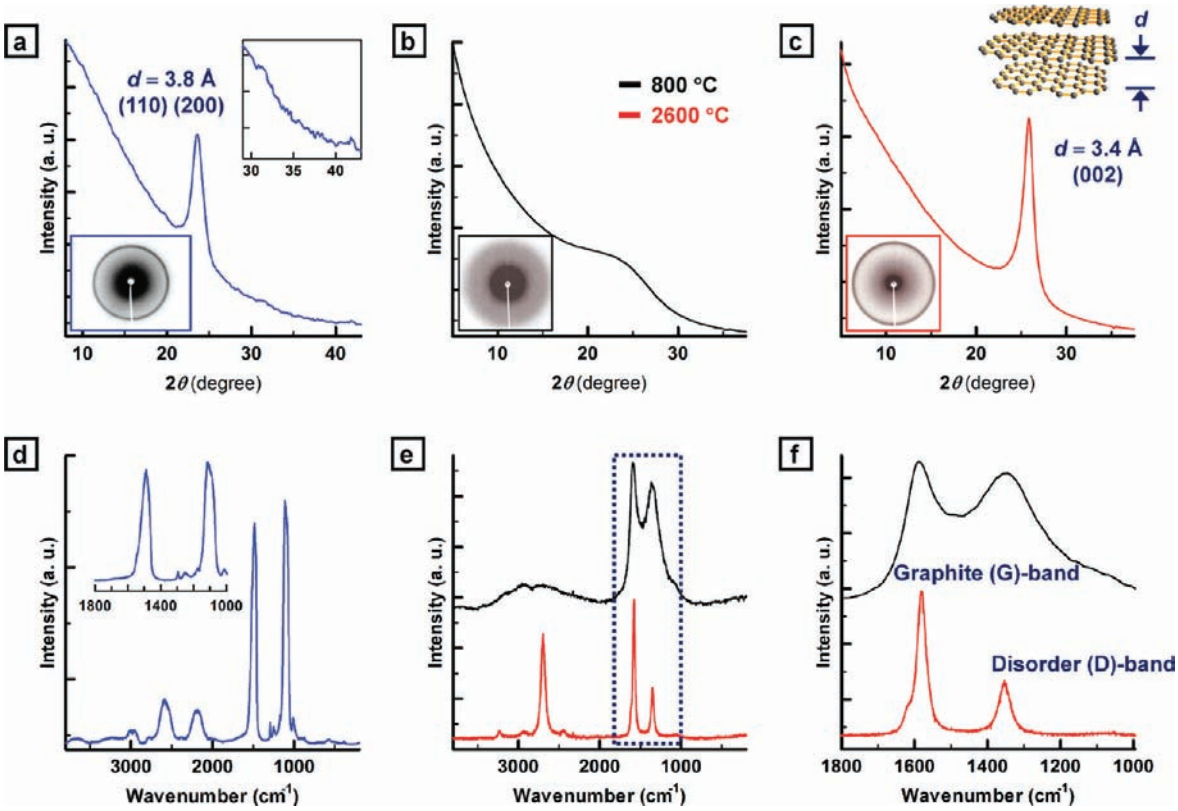

Figure 9. (a) Typical XRD profile of the PA film. The inset shows the XRD pattern of the PA film. The XRD profile for the film (b) carbonized at 800 °C (black) and (c) heat-treated at 2600 °C after the carbonization (red). The insets show the XRD patterns of (b) carbon and (c) graphite films prepared by the morphology-retaining carbonization. (d) Typical Raman-scattering spectrum of the PA film and its magnified spectrum. (e) Raman-scattering spectra of the carbon (black) and graphite (red) films and (f) their magnified spectra.

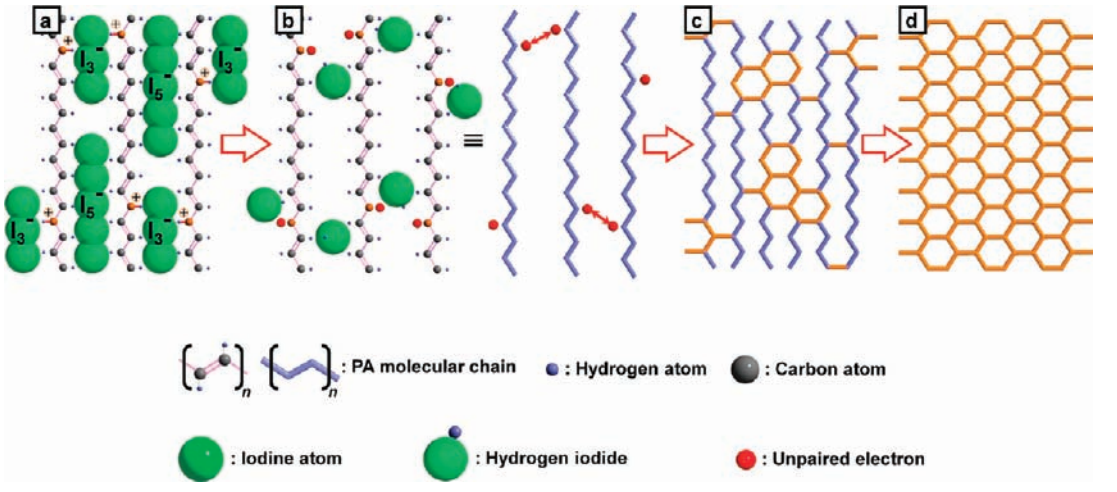

Figure 10. (a) Structural model of iodine-doped PA. (b) Removal of hydrogen as hydrogen iodide from the PA chain. (c) Hypothetical molecular model of the specimen formed on route to the dehydrogenation reaction from the iodine-doped PA film. (d) Hexagonal carbon-bond network formed at 800 °C after passing through the model shown in panel c.

using the N*-LC of system 1 (see Table 1). A spiral morphology consisting of helical bundles of fibrils is observed in a domain. The yield of the carbon film after the carbonization at 800 °C is as high as 71−90% of the weight of the H-PA film before iodine doping. It is worth noting that the carbon film prepared from undoped H-PA preserves neither its fibrous structure nor its spiral morphology after the carbonization at 800 °C. A black char less than 30% in weight remained at temperature above 800 °C in the form of particles (Figure 6a). This char is due to the thermal decomposition usually encountered in the carbonization of organic films. The helical carbon films prepared using the H-PAs, synthesized in N*-LCs including the chiral dopants of (*R*)- and (*S*)-configurations, exhibit screwed bundle of fibrils with left- and right-hand directions, respectively

dx.doi.org/10.1021/ja2082922 |*J. Am. Chem. Soc.* 2011, 133, 17977–17992

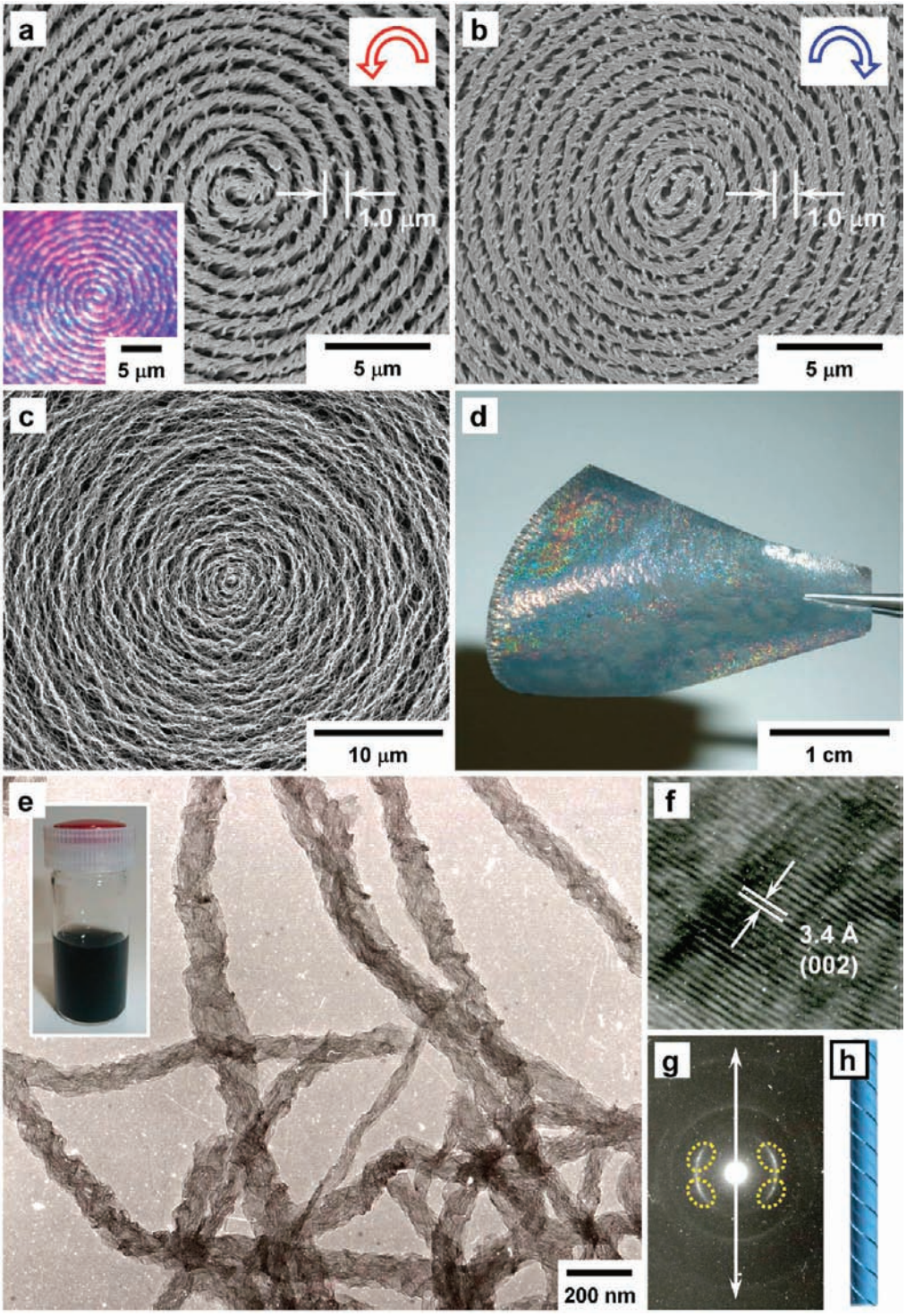

Figure 11. SEM image of the helical graphite films with spiral morphology prepared by carbonization and then heat treatment at 2600 °C for H-PAs that were synthesized in N*-LCs, including (a) (*R*)-D1 [system 1], (b) (*S*)-D1 [system 1], and (c) (*R*)-D3 [system 4]. The inset shows the DICM image of the helical graphite film. (d) Photograph of the freestanding graphite film with structural color. (e) TEM image of the dispersed helical graphitic fibrils prepared through the graphitization of H-PA film synthesized in the (*R*)-N*-LC of system 4 and (f) the corresponding high-resolution TEM image of the helical graphite fibrils. The inset shows a photograph of the well-dispersed helical graphitic fibrils in ethanol. (g) SAED pattern showing two pairs of the (002) reflection of the helical graphitic fibril. The four dotted circles drawn in the image indicate the positions of the two pairs' reflections. An arrow indicates the direction of the fiber axis. (h) Schematic representation of the helical graphitic fibril.

(Figure 6c and d). Therefore it can be argued that the screw directions of the carbon fibrils can be controlled by choosing chirality of the chiral dopant.[16a,c]

Figure 7b shows the SEM image of the helical carbon film with spiral morphology prepared using (*S*)-N*-LC of system 2 (see Table 1). It is clear that the bundles of the helical carbon fibrils are

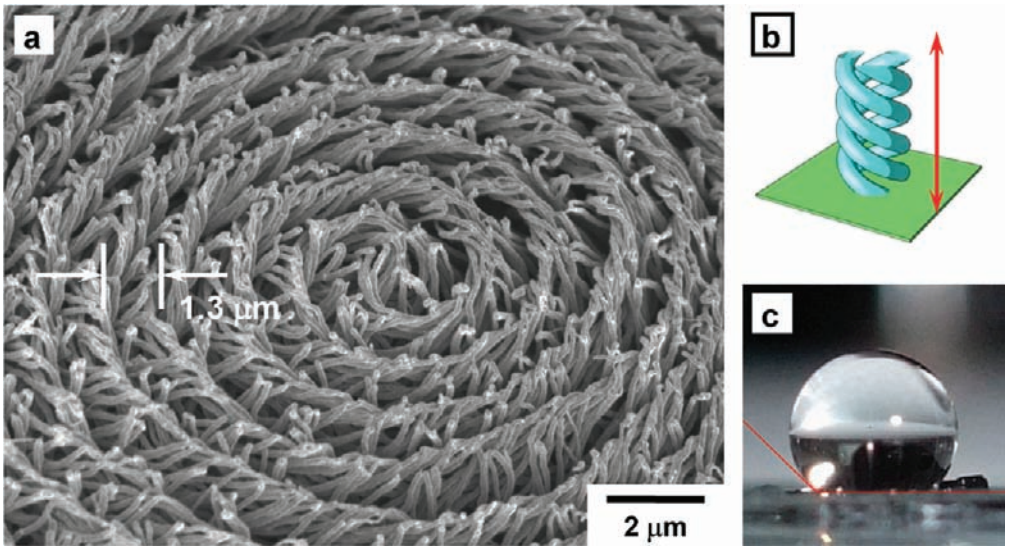

Figure 12. (a) SEM image of the left-handed helical carbon film with vertically aligned morphology prepared using H-PA synthesized in the (*R*)-N*-LC of system 3. (b) Schematic representation of the vertically aligned helical carbon. (c) Photograph of a drop of water on the surface of the vertically aligned helical carbon film that has water-repellent property.

highly twisted in the right-hand direction. The addition of a small amount of D2 (0.5 mol %) into a N-LC enabled us to prepare a highly twisted helical carbon film; the molar concentration of D2 in system 2 is less than one-quarter that of D1 in system 1. This situation is attributed to the HTP (β_M) of D2 being 154−160 μm^{-1}, which is much larger than that of D1 ($\beta_M = 46\ \mu m^{-1}$) in system 1, resulting in a highly twisted N*-LC despite the lower concentration of D2 in system 2. The hierarchical helical structure was also observed in the resultant carbon film.

3.5. Helical Carbon Films with Bundle-Free Fibrils. Figures 7c and 8 show micrographs of the helical carbon film prepared using (*R*)-N*-LC of system 4 (see Table 1). System 4 is a highly twisted N*-LC with a helical pitch of 260−270 nm due to the influence of a ultimately twisted chiral dopant, such as tetra-substituted binaphthyl derivative, D3, whose HTP (247−256 μm^{-1}) is larger than that (154−160 μm^{-1}) of D2. Figure 7c shows that the helical carbon film has left-handed fibrils but no fibril bundles, which is in stark contrast to the morphology of the other helical carbon films prepared using systems 1 and 2. This morphology difference can be explained as follows. In the moderately twisted N*-LCs (systems 1 and 2) whose helical pitches are larger than 1 μm (2.2−2.6 μm), the fibrils of the H-PA film are gathered to form bundles. However, in the ultimately twisted N*-LC (system 4) whose helical pitch is much smaller than 1 μm (260−270 nm), the H-PA film has highly screwed fibrils but cannot form bundles of the fibrils because of the very narrow helical pitches of the N*-LC.

Figure 8b and c show the top- and isometric-view SEM images of the helical carbon film, respectively. The diameters of the spiral domains are less than 70 μm. Owing to the hierarchical morphology, the highly twisted helical carbon film has a spherulitic multidomain morphology, as shown in the lower-left inset of Figure 8a. The bundle-free morphology might be useful in evaluating the inherent electromagnetic properties of the single-screwed fibril.[16f] From the experimental results mentioned above, it is confirmed that the spiral morphology of the helical carbon film crucially depends on the chirality and HTP of the chiral dopant (Figure 7).

3.6. XRD Intensity Curves and Raman Scattering Spectra. Figure 9a depicts the X-ray diffraction (XRD) pattern of the PA film and the magnified pattern. The pattern shows sharp (110) and (200) reflections at 3.8 Å (23.6° in 2θ), a (210) reflection at 3.0 Å (30.9° in 2θ), and a (002) reflection at 2.2 Å (41.8° in 2θ). This indicates that the PA thin film has a highly crystalline region inside the fibril.[28,29] The Raman spectrum of the PA film is shown in Figure 9d. The spectrum for the PA thin film has two large peaks at about 1500 and 1100 cm^{-1}, which are assigned to the C═C stretching vibration and the mixed vibration of C−C stretching and C−H in-plane bending of *trans*-PA, respectively.[30]

The XRD of the carbon film prepared from the iodine-doped PA film at 800 °C has no crystalline reflection (Figure 9b). However, the Raman spectrum of the carbon film shows a broad peak at 1350 cm^{-1} that is attributed to the disordered structure (D-band) and a stronger peak at 1580 cm^{-1} corresponding to the structure of the sp^2 hexagonal carbon network (G-band) (Figure 9e and f).[1]

It is clear that the iodine doping prevents the H-PA film from thermally decomposing at high temperature. According to the structural model of the iodine-doped H-PA film,[31] polyiodide ions such as I_3^- and I_5^- are situated between the H-PA chains to form charge-transfer complexes (Figure 10a). Iodine tends to react with hydrogen at high temperatures.[32] Because an outgassing of hydrogen iodide has been detected by gas chromatography−mass spectrometry (GC−MS) during the heating of the doped H-PA film, it can be assumed that the hydrogen atoms contained in the doped H-PA are removed to some extent as hydrogen iodide from the H-PA chain (Figure 10b) and that the H-PA chains partially cross-link between the adjacent chains (Figure 10c). Thus, most of the hydrogens are removed from the H-PA main chain with further heating. Consequently, the networks of sp^2 hexagonal carbon bonds are formed during carbonization (Figure 10d). The thermal behaviors of the undoped and doped PA films during carbonization were also examined using thermogravimetry and differential thermal analysis (TG-DTA). Experimental details are described in the Supporting Information (Figure S8). These results imply that the helical

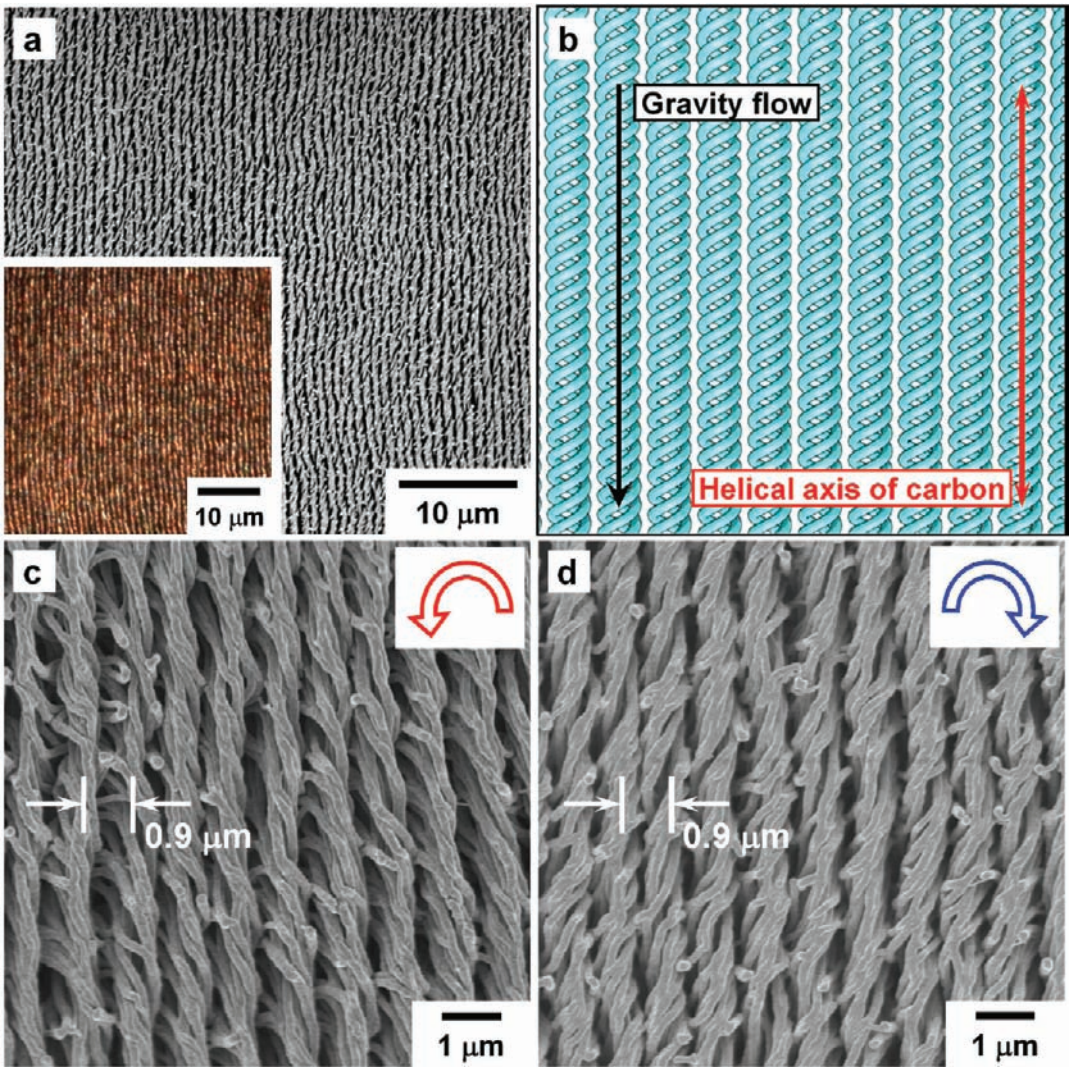

Figure 13. (a) SEM image of the horizontally aligned helical carbon film prepared using H-PA synthesized in the (*S*)-N*-LC of system 2. The inset shows the DICM image of the helical carbon film. (b) Schematic representation of the horizontally aligned helical carbon. SEM images of the (c) left- and (d) right-handed helical carbon films with horizontally aligned morphologies prepared by the carbonization at 800 °C for H-PAs that were synthesized in N*-LC using (c) (*R*)- and (d) (*S*)-D2 [system 2], respectively.

carbon film prepared from the doped H-PA film at 800 °C exists in an almost amorphous state.

The carbon film prepared at 800 °C was further graphitized by heat treatment at 2600 °C. The two Raman bands at 1350 and 1580 cm^{-1} become sharp, and at the same time the former and the latter decrease and increase in intensity, respectively (Figure 9e and f). The sharp XRD peak corresponding to the (002) plane of a graphitic crystal[2] indicates that the graphitic crystallization further proceeds in the carbon film through the heat treatment at 2600 °C (Figure 9c). The sharp peak of the graphite film, 26.0° in 2θ, was evaluated to be 3.4 Å. It should be emphasized that the graphite film prepared by the heat treatment at 2600 °C (Figure 11a−d and Figure S9 in Supporting Information) has almost the same helical structure as that of the original H-PA film and that of the helical carbon film prepared at 800 °C (Figures 2−8). Note that although the natural color of the H-PA, helical carbon, and helical graphite films are dark gray or black, the films exhibited structural color upon irradiation with white light. This is due to their hierarchical structure composed of the fibril bundles (Figure 11d and Figure S10 in Supporting Information).

3.7. TEM Images of Helical Graphitic Fibrils. Transmission electron microscopy (TEM) measurements indicate that ultrasonication of the helical graphite film gives rise to a single helical graphite fibril. Ultrasonication was applied to a small piece of the helical graphite film immersed in ethanol (EtOH) for several hours to separate the fibril bundle of the film (Figure 11e, inset). The TEM image of the dispersed helical graphitic fibrils is given in Figure 11e, and the high-resolution TEM image is given in Figure 11f. The interplanar distance of 3.4 Å corresponds to the distance between the hexagonal carbon layers. Figure 11g shows a typical selected-area electron-diffraction (SAED) pattern of the single helical graphitic fibril. SAED pattern of the single helical graphite fibril shows two pairs of the (002) reflection of the graphitic crystals[2] with an intersection angle in the range of 45−60° along the fibril axis. Figure 11h shows a schematic representation of a single helical graphitic fibril, which can be deduced from the SEM and TEM images and SAED profiles.[23]

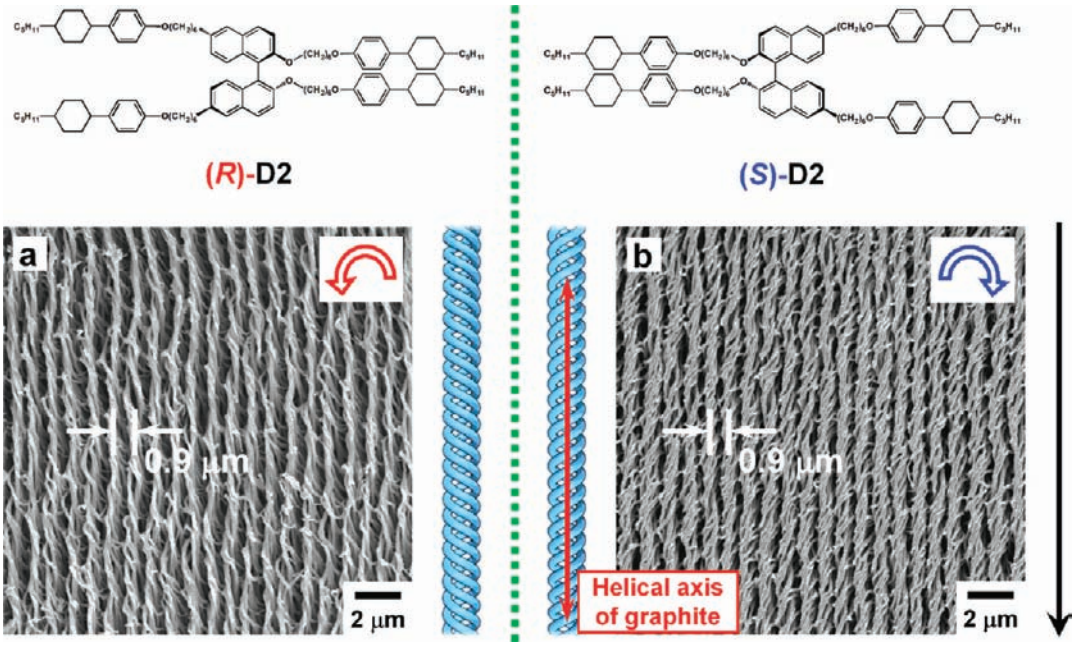

Figure 14. SEM images of (a) left- and (b) right-handed helical graphite films with horizontally aligned morphologies prepared by carbonization and then heat treatments at 2600 °C for H-PAs that were synthesized in N*-LC using (a) (*R*)- and (b) (*S*)-D2 [system 2], respectively. The black arrow indicates the direction of the gravity flow.

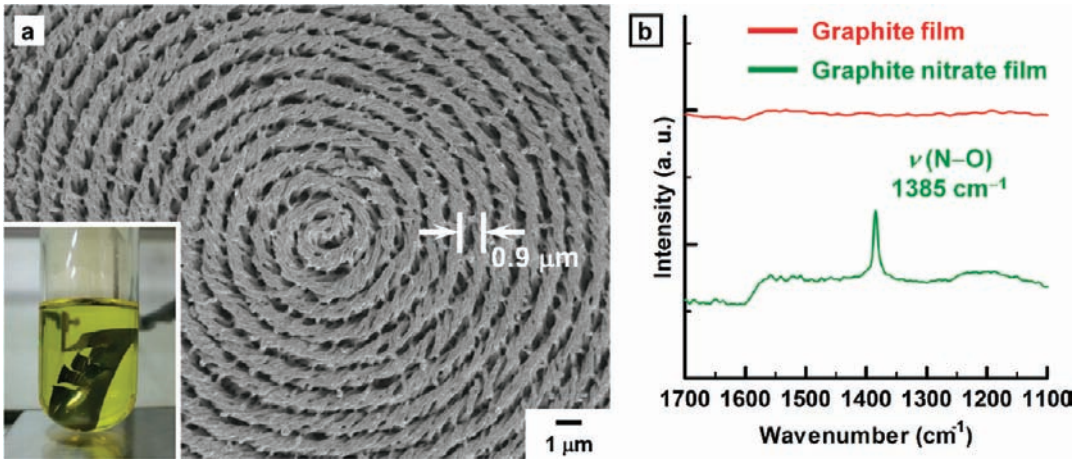

Figure 15. (a) SEM image of helical graphite nitrate film doped with fuming HNO_3 [$C_{68}^{+}(NO_3^{-})$]. The helical graphite film was prepared by carbonization and then heat treatment at 2600 °C for H-PA that was synthesized in N*-LC using (*R*)-D1 [system 1]. The inset shows the graphite film immersed in fuming HNO_3. (b) IR spectra of the graphite and the graphite nitrate films. The absorption peak of 1385 cm^{-1} is attributed to N—O vibration of the NO_3^{-} ion.[34]

3.8. Vertical and Horizontal Alignments. Figure 12a shows the SEM image of the vertically aligned helical carbon film prepared using the iodine-doped H-PA films synthesized in the (*R*)-N*-LC of system 3 (see Table 1). The fibril bundle of the helical carbon are vertically aligned and highly twisted in the left-hand direction (Figure 12b). Interestingly, the vertically aligned carbon film plays the role of a hydrophobic substrate. Because the carbon film has both a fibril structure and a vertically aligned morphology, it is anticipated to show water-repellent property. The optical image of the carbon film with a drop of water (Figure 12c) reveals a contact angle of around 136°, depending on the sample. It is notable that the surface is hydrophobic without any further surface treatment for lowering the surface energy.

The horizontally aligned H-PA films were synthesized in the N*-LC composed of system 2 with a monodomain structure using the gravity-flow method.[19] The gravity flow enabled us to achieve a highly ordered macroscopic orientation of the N*-LC in a few minutes of orientation time (Figure 5a, inset). The H-PA films exhibit highly aligned helical bundles of fibrils, as shown in Figure 5c and d. The horizontally aligned helical carbon films were prepared through the carbonization of the aligned H-PA films at 800 °C after iodine doping. Figure 13 shows the SEM and DICM images of the horizontally aligned helical carbon films prepared from iodine-doped horizontally aligned H-PA films.

Furthermore, the horizontally aligned helical graphite films were then prepared through the subsequent heating of the carbon

films at 2600 °C. Figure 14 shows the SEM images of the screw-direction-controlled helical graphitic fibrils with a horizontally aligned morphology. The helical graphite films prepared using the horizontally aligned H-PA films, synthesized in the macroscopically oriented N*-LCs of system 2 including the chiral dopants of (*R*)- and (*S*)-D2, exhibit screwed fibril bundles with left- and right-hand directions, respectively. It is clear that the screwed fibril bundles are aligned parallel to the direction of the gravity flow (Figure S11 in Supporting Information). This finding is in stark contrast to the spiral helical graphite films prepared from the concentrically curled H-PA films that were synthesized in N*-LCs composed of system 2 with a multidomain structure. The aligned helical graphite film has not only helically screwed but also horizontally aligned fibril bundles. It is anticipated that the macroscopically aligned helical graphite film might be available for carbon materials with induced solenoid magnetism.

3.9. Electrical Conductivities of Helical Carbon and Graphite Films. Lastly, it is worthwhile to remark that although the original undoped H-PA film has an electrical conductivity of less than 10^{-5} S/cm at room temperature,[33] the helical carbon and graphite films have conductivities on the order of 10 and 10^2 S/cm, respectively, without doping. The conductivity of the graphite film was increased by several times through the doping with fuming nitric acid (HNO_3). HNO_3 doping was performed by immersing the helical graphite film in fuming HNO_3 in a Schlenk flask at room temperature for over 24 h (inset of Figure 15a). The amount of dopant was determined by weighing the doped helical graphite films. The atomic ratio of carbon to doped NO_3^- in the helical graphite film (C/NO_3) was about 68. The doped graphite film retains its helical morphology throughout the doping (Figure 15a). Figure 15b shows typical IR absorption spectra of the graphite and the graphite nitrate films. The absorption peak of 1385 cm^{-1} provides an evidence for that a NO_3^- ion is formed as a dopant species in the graphite film.[34] Furthermore, the carbon and graphite films prepared from the horizontally aligned H-PA film exhibit an enhancement in the electrical conductivity and an evolution of electrical anisotropy, where the conductivity parallel ($\sigma_{\parallel}$) to the helical axis of the fibril bundle is higher than that ($\sigma_{\perp}$) perpendicular to the axis. The electrical anisotropy, defined as the parallel-to-perpendicular value of conductivity ($\sigma_{\parallel}/\sigma_{\perp}$), is 1.5−2.0, depending on the sample. This value is nearly equal to the values of the original H-PA films (Figure S4 in Supporting Information). The unexpectedly small anisotropy is attributed to closely neighboring fibrils due to the helical structure, which increases the perpendicular conductivity through interfibril hoppings of charged carriers and diagonal transportation passes.

4. CONCLUSIONS

The carbonization of H-PA films via iodine doping was found to produce hierarchically controlled helical carbon films, where the concentrically curled or macroscopically aligned morphologies and even helical fibril structures were completely preserved. The carbon film prepared by carbonization at 800 °C can be graphitized by subsequent heating at 2600 °C while retaining the morphology, when the iodine-doped H-PA is employed as a precursor of the carbonization and graphitization. Furthermore, the screw direction, twist degree, and macroscopic alignment of the helical graphite film are rigorously controlled by changing the helical sense, helical pitch, and orientation of N*-LC used as asymmetric reaction field for the synthesis of the H-PA films.

The PA films are generally unstable under atmospheric conditions, irrespective of being pristine or doped films because PA conjugated bonds tend to react easily with oxygen due to its low ionization potential. This is the reason why the PA films are less feasible for practical use. However, the hierarchically controlled helical graphite films prepared using the present method are quite stable under atmospheric conditions. It is therefore expected that the graphite films will exhibit intrinsic functions and performances characteristic of the helical structure, and their morphologies bearing bundle-free fibrils or macroscopically aligned helical fibrils might be useful for exploring the properties of helical graphite fibrils that are still not cultivated before.

■ ASSOCIATED CONTENT

Supporting Information. Materials, measurements, acetylene polymerizations, and the effect of iodine doping. This material is available free of charge via the Internet at http://pubs.acs.org.

■ AUTHOR INFORMATION

Corresponding Author
akagi@fps.polym.kyoto-u.ac.jp

■ ACKNOWLEDGMENT

We would like to thank Dr. Y. Matsui, Dr. T. Nagai, and Dr. M. Nagao (NIMS, Japan) for the TEM measurements, Dr. A. Kaito and Dr. M. Shimomura (AIST, Japan) for the Raman spectra measurements, and Dr. S. Ohshima and Dr. T. Saito (AIST, Japan) for the use of the graphitizing apparatus. The authors are also grateful to laboratory colleagues Dr. T. Mori (current address: NIMS, Japan) and Dr. M. Goh, Department of Polymer Chemistry, Kyoto University and Mr. T. Noguchi, Institute of Materials Science, University of Tsukuba for their helpful advice in synthesizing H-PA films. This work was supported by a Grant-in-Aid for Science Research (S) (No. 20225007) and one for Challenging Exploratory Research (No. 21651043) from the Ministry of Education, Culture, Sports, Science and Technology, Japan.

■ REFERENCES

(1) *Carbon: The Future Materials for Advanced Technology Applications*; Messina, G., Santangelo, S., Eds.; Springer: Heidelberg, 2005.

(2) *New Carbon: Control of Structure and Functions*; Inagaki, M., Ed.; Elsevier: Amsterdam, 2000.

(3) Centrone, A.; Brambilla, L.; Zerbi, G. *Phys. Rev. B* **2005**, *71*, 245406-1–245406-7.

(4) (a) Wu, J.; Pisula, W.; Müllen, K. *Chem. Rev.* **2007**, *107*, 718–747. (b) Wang, X.; Zhi, L.; Müllen, K. *Nano Lett.* **2008**, *8*, 323–327. (c) Zhi, L.; Müllen, K. *J. Mater. Chem.* **2008**, *18*, 1472–1484. (d) Wang, X.; Zhi, L.; Tsao, N.; Tomović, Ž.; Li, J.; Müllen, K. *Angew. Chem., Int. Ed.* **2008**, *47*, 2990–2992.

(5) Thompson, B. C.; Fréchet, J. M. J. *Angew. Chem., Int. Ed.* **2008**, *47*, 58–77.

(6) (a) Ahn, Y. H.; Tsen, A. W.; Kim, B.; Park, Y. W.; Park, J. *Nano Lett.* **2007**, *7*, 3320–3323. (b) Gilje, S.; Han, S.; Wang, M.; Wang, K. L.; Kaner, R. B. *Nano Lett.* **2007**, *7*, 3394–3398.

(7) Adelhelm, P.; Hu, Y.-S.; Chuenchom, L.; Antonietti, M.; Smarsly, B. M.; Maier, J. *Adv. Mater.* **2007**, *19*, 4012–4017.

(8) (a) Miyake, K.; Kusunoki, M.; Usami, H.; Umehara, N.; Sasaki, S. *Nano Lett.* **2007**, *7*, 3285–3289. (b) Sethi, S.; Ge, L.; Ci, L.; Ajayan, P. M.; Dhinojwala, A. *Nano Lett.* **2008**, *8*, 822–825.

(9) (a) Stankovich, S.; Dikin, D. A.; Dommett, G. H. B.; Kohlhaas, K. M.; Zimney, E. J.; Stach, E. A.; Piner, R. D.; Nguyen, S. T.; Ruoff, R. S. *Nature* **2006**, *442*, 282–286. (b) Li, D.; Müller, M. B.; Gilje, S.; Kaner, R. B.; Wallace, G. G. *Nat. Nanotechnol.* **2007**, *3*, 101–105. (c) Geim, A. K.; Novoselov, K. S. *Nat. Mater.* **2007**, *6*, 183–191.

(10) (a) Zhang, M.; Fang, S.; Zakhidov, A. A.; Lee, S. B.; Aliev, A. E.; Williams, C. D.; Atkinson, K. R.; Baughman, R. H. *Science* **2005**, *309*, 1215–1219. (b) Simmons, T. J.; Hashim, D.; Vajtai, R.; Ajayan, P. M. *J. Am. Chem. Soc.* **2007**, *129*, 10088–10089. (c) Kaiser, A. B.; Skákalová, V.; Roth, S. *Phys. Status Solidi B* **2007**, *244*, 4199–4203. (d) Ding, L.; Yuan, D.; Liu, J. *J. Am. Chem. Soc.* **2008**, *130*, 5428–5429. (e) Baca, A. J.; Ahn, J.-H.; Sun, Y.; Meitl, M. A.; Menard, E.; Kim, H.-S.; Choi, W. M.; Kim, D.-H.; Huang, Y.; Rogers, J. A. *Angew. Chem., Int. Ed.* **2008**, *47*, 5524–5542. (f) LeMieux, M. C.; Roberts, M.; Barman, S.; Jin, Y. W.; Kim, J. M.; Bao, Z. *Science* **2008**, *321*, 101–104.

(11) *Thermal Degradation of Polymeric Materials*; Pielichowski, K., Niuguna, J., Eds.; Rapra Technology: Shropshire, U.K., 2005.

(12) (a) Amabilino, D. B.; Stoddart, J. F. *Chem. Rev.* **1995**, *95*, 2725–2828. (b) Hill, J. P.; Jin, W.; Kosaka, A.; Fukushima, T.; Ichihara, H.; Shimomura, T.; Ito, K.; Hashizume, T.; Ishii, N.; Aida, T. *Science* **2004**, *304*, 1481–1483. (c) Shimizu, T.; Masuda, M.; Minamikawa, H. *Chem. Rev.* **2005**, *105*, 1401–1443. (d) Yang, Y.-W.; Lee, E.; Lee, M. *J. Am. Chem. Soc.* **2006**, *128*, 3484–3485. (e) Palmer, L. C.; Stupp, S. I. *Acc. Chem. Res.* **2008**, *41*, 1674–1684.

(13) (a) Berl, V.; Huc, I.; Khoury, R. G.; Krische, M. J.; Lehn, J.-M. *Nature* **2000**, *407*, 720–723. (b) Katz, T. J. *Angew. Chem., Int. Ed.* **2000**, *39*, 1921–1923. (c) Hill, D. J.; Mio, M. J.; Prince, R. B.; Hughes, T. S.; Moore, J. S. *Chem. Rev.* **2001**, *101*, 3893–4011. (d) Hoeben, F. J. M.; Jonkheijm, P.; Meijer, E. W.; Schenning, A. P. H. J. *Chem. Rev.* **2005**, *105*, 1491–1546. (e) Ajayaghosh, A.; Praveen, V. K. *Acc. Chem. Res.* **2007**, *40*, 644–656.

(14) (a) Green, M. M.; Zanella, S.; Gu, H.; Sato, T.; Gottarelli, G.; Jha, S. K.; Spada, G. P.; Schoevaars, A. M.; Feringa, B.; Teramoto, A. *J. Am. Chem. Soc.* **1998**, *120*, 9810–9817. (b) Green, M. M.; Park, J.-W.; Sato, T.; Teramoto, A.; Lifson, S.; Selinger, R. L. B.; Selinger, J. V. *Angew. Chem., Int. Ed.* **1999**, *38*, 3138–3154. (c) Tang, K.; Green, M. M.; Cheon, K. S.; Selinger, J. V.; Garetz, B. A. *J. Am. Chem. Soc.* **2003**, *125*, 7313–7323. (d) Pijper, D.; Jongejan, M. G. M.; Meetsma, A.; Feringa, B. L. *J. Am. Chem. Soc.* **2008**, *130*, 4541–4552.

(15) (a) McQuade, D. T.; Pullen, A. E.; Swager, T. M. *Chem. Rev.* **2000**, *100*, 2537–2574. (b) Cornelissen, J. J. L. M.; Rowan, A. E.; Nolte, R. J. M.; Sommerdijk, N. A. J. M. *Chem. Rev.* **2001**, *101*, 4039–4070. (c) Hatano, T.; Bae, A.-H.; Takeuchi, M.; Fujita, N.; Kaneko, K.; Ihara, H.; Takafuji, M.; Shinkai, S. *Angew. Chem., Int. Ed.* **2004**, *43*, 465–469. (d) Masuda, T. *J. Polym. Sci., Part A: Polym. Chem.* **2007**, *45*, 165–180. (e) Liu, J.; Lam, J. W. Y.; Tang, B. Z. *Chem. Rev.* **2009**, *109*, 5799–5867. (f) Rosen, B. M.; Wilson, C. J.; Wilson, D. A.; Peterca, M.; Imam, M. R.; Percec, V. *Chem. Rev.* **2009**, *109*, 6275–6540.

(16) (a) Akagi, K.; Piao, G.; Kaneko, S.; Sakamaki, K.; Shirakawa, H.; Kyotani, M. *Science* **1998**, *282*, 1683–1686. (b) Lee, H. J.; Jin, Z. X.; Aleshin, A. N.; Lee, J. Y.; Goh, M. J.; Akagi, K.; Kim, Y. S.; Kim, D. W.; Park, Y. W. *J. Am. Chem. Soc.* **2004**, *126*, 16722–16723. (c) Akagi, K.; Guo, S.; Mori, T.; Goh, M.; Piao, G.; Kyotani, M. *J. Am. Chem. Soc.* **2005**, *127*, 14647–14654.(d) Akagi, K. Helical Polyacetylene Synthesized in Chiral Nematic Liquid Crystal. In *Handbook of Conducting Polymers, Conjugated Polymers: Theory, Synthesis, Properties, and Characterization*, 3rd ed.; Skotheim, T. A., Reynolds, J. R., Eds.; CRC Press: New York, 2007; pp 3-3−3-14. (e) Akagi, K. *Polym. Int.* **2007**, *56*, 1192–1199. (f) Goh, M.; Kyotani, M.; Akagi, K. *J. Am. Chem. Soc.* **2007**, *129*, 8519–8527. (g) Goh, M.; Matsushita, T.; Kyotani, M.; Akagi, K. *Macromolecules* **2007**, *40*, 4762–4771. (h) Mori, T.; Kyotani, M.; Akagi, K. *Macromolecules* **2008**, *41*, 607–613. (i) Akagi, K.; Mori, T. *Chem. Rec.* **2008**, *8*, 395–406. (j) Akagi, K. *Chem. Rev.* **2009**, *109*, 5354–5401. (k) Goh, M.; Matsushita, S.; Akagi, K. *Chem. Soc. Rev.* **2010**, *39*, 2466–2476.

(17) (a) Solladié, G.; Zimmermann, R. G. *Angew. Chem., Int. Ed.* **1984**, *23*, 348–362. (b) Pieraccini, S.; Ferrarini, A.; Spada, G. P. *Chirality* **2008**, *20*, 749–759.

(18) *Chirality in Liquid Crystals*; Kitzerow, H. S., Bahr, C., Eds.; Springer: New York, 2001.

(19) (a) Araya, K.; Mukoh, A.; Narahara, T.; Shirakawa, H. *Chem. Lett.* **1984**, 1141–1142. (b) Araya, K.; Mukoh, A.; Narahara, T.; Shirakawa, H. *Synth. Met.* **1986**, *14*, 199–206. (c) Akagi, K.; Shirakawa, H.; Araya, K.; Mukoh, A.; Narahara, T. *Polym. J.* **1987**, *19*, 185–189. (d) Araya, K.; Mukoh, A.; Narahara, T.; Akagi, K.; Shirakawa, H. *Synth. Met.* **1987**, *17*, 247–252. (e) Kyotani, M.; Matsushita, S.; Goh, M.; Nagai, T.; Matsui, Y.; Akagi, K. *Nanoscale* **2010**, *2*, 509–514.

(20) (a) Akagi, K.; Katayama, S.; Shirakawa, H.; Araya, K.; Mukoh, A.; Narahara, T. *Synth. Met.* **1987**, *17*, 241–246. (b) Shirakawa, H.; Akagi, K.; Katayama, S.; Araya, K.; Mukoh, A.; Narahara, T. *J. Macromol. Sci., Chem.* **1988**, *A25*, 643–654. (c) Akagi, K.; Katayama, S.; Ito, M.; Shirakawa, H.; Araya, K. *Synth. Met.* **1989**, *28*, D51–D56. (d) Akagi, K.; Ito, M.; Katayama, S.; Shirakawa, H. *Mol. Cryst. Liq. Cryst.* **1989**, *172*, 115–123.

(21) (a) Shirakawa, H.; Otaka, T.; Piao, G.; Akagi, K.; Kyotani, M. *Synth. Met.* **2001**, *117*, 1–8. (b) Piao, G.; Otaka, T.; Sato, T.; Akagi, K.; Kyotani, M. *Mol. Cryst. Liq. Cryst.* **2001**, *365*, 117–127. (c) Mori, T.; Sato, T.; Kyotani, M.; Akagi, K. *Macromolecules* **2009**, *42*, 1817–1823.

(22) Kyotani, M.; Matsushita, S.; Nagai, T.; Matsui, Y.; Akagi, K. *Synth. Met.* **2007**, *157*, 546–550.

(23) (a) Kyotani, M.; Matsushita, S.; Nagai, T.; Matsui, Y.; Shimomura, M.; Kaito, A.; Akagi, K. *J. Am. Chem. Soc.* **2008**, *130*, 10880–10881. (b) Matsushita, S.; Kyotani, M.; Akagi, K. *Synth. Met.* **2009**, *159*, 2198–2201.

(24) Kanazawa, K.; Higuchi, I.; Akagi, K. *Mol. Cryst. Liq. Cryst.* **2001**, *364*, 825–834.

(25) (a) Isaert, N.; Soulestin, B.; Malthete, J. *Mol. Cryst. Liq. Cryst.* **1976**, *37*, 321–333. (b) Gray, G. W.; McDonnell, D. G. *Mol. Cryst. Liq. Cryst.* **1977**, *34*, 211–217.

(26) (a) Grandjean, F. *C. R. Hebd. Seances Acad. Sci.* **1921**, *172*, 71–74. (b) Cano, R. *Bull. Soc. Fr. Mineral Cristallogr.* **1968**, *91*, 20–27. (c) Sagisaka, T.; Yokoyama, Y. *Bull. Chem. Soc. Jpn.* **2000**, *73*, 191–196.(d) *Textures of Liquid Crystals*; Dierking, I., Ed.; Wiley-VCH: Weinheim, 2003.

(27) (a) Friedel, G. *Ann. Phys.* **1922**, *18*, 273–474. (b) Fergason, J. L. *Mol. Cryst.* **1966**, *1*, 293–307.

(28) Akaishi, T.; Miyasaka, K.; Ishikawa, K.; Shirakawa, H.; Ikeda, S. *J. Polym. Sci., Polym. Phys. Ed.* **1980**, *18*, 745–750.

(29) Montaner, A.; Rolland, M.; Sauvajol, J. L.; Galtier, M.; Almairac, R.; Ribet, J. L. *Polymer* **1988**, *29*, 1101–1104.

(30) Arbuckle, G. A.; Buecheler, N. M.; Hall, J. W.; Valentine, K. G.; Lefrant, S.; Mevellec, J. Y.; Mulazzi, E. *Synth. Met.* **1996**, *79*, 183–188.

(31) (a) Roth, S.; Bleier, H. *Adv. Phys.* **1987**, *36*, 385–462. (b) Perego, G.; Lugli, G.; Pedretti, U.; Alligra, G. *Makromol. Chem.* **1988**, *189*, 2687–2701.

(32) *Encyclopedia of Industrial Chemical Analysis*; Snell, F. D., Ettre, L. S., Eds.; Interscience Publishers: New York, 1971.

(33) (a) Heeger, A. J. *Rev. Mod. Phys.* **2001**, *73*, 681–700. (b) MacDiarmid, A. G. *Rev. Mod. Phys.* **2001**, *73*, 701–712. (c) Shirakawa, H. *Rev. Mod. Phys.* **2001**, *73*, 713–718.

(34) *Infrared and Raman Spectra of Inorganic and Coordination Compounds*, 4th ed.; Nakamoto, K., Ed.; John Wiley & Sons: New York, 1986.